APL Photonics

High efficiency four wave mixing and optical bistability in amorphous silicon carbide ring resonators

Cite as: APL Photonics **5**, 076110 (2020); https://doi.org/10.1063/5.0009692
Submitted: 15 April 2020 • Accepted: 06 July 2020 • Published Online: 21 July 2020

Peng Xing, Danhao Ma, Lionel C. Kimerling, et al.

High efficiency four wave mixing and optical bistability in amorphous silicon carbide ring resonators

Cite as: APL Photon. 5, 076110 (2020); doi: 10.1063/5.0009692
Submitted: 15 April 2020 • Accepted: 6 July 2020 •
Published Online: 21 July 2020

Peng Xing,[1] Danhao Ma,[2] Lionel C. Kimerling,[2,3] Anuradha M. Agarwal,[2,3] and Dawn T. H. Tan[1,a)]

AFFILIATIONS

[1]SUTD-MIT International Design Center, Singapore University of Technology and Design, 8 Somapah Road, Singapore, 489627
[2]Department of Materials Science and Engineering, Massachusetts Institute of Technology, Cambridge, Massachusetts 02139, USA
[3]Materials Research Laboratory, Massachusetts Institute of Technology, Cambridge, Massachusetts 02139, USA

[a)]**Author to whom correspondence should be addressed:** dawn_tan@sutd.edu.sg

ABSTRACT

We demonstrate high efficiency wavelength conversion via four wave mixing in amorphous silicon carbide ring resonators with a loaded quality factor of 70 000. Owing to the high quality factor and high nonlinearity of amorphous silicon carbide, −21 dB conversion efficiency is achieved with 15 mW pump power. Moreover, the thermo-optic coefficient (TOC) of amorphous silicon carbide is measured to be $1.4 \times 10^{-4}/^{\circ}\mathrm{C}$ at telecommunication wavelengths. Taking advantage of the high TOC, we demonstrate optical bistability in the silicon carbide ring resonator. This work presents amorphous silicon carbide as a promising platform for applications in optical signal processing.

INTRODUCTION

Advances in nonlinear integrated optics have boosted applications in areas such as all-optical signal processing, all-optical switching, and quantum optics. Since the nonlinear process efficiency is highly dependent on the material nonlinearity, materials with high nonlinearity are sought after. Silicon has been assessed by numerous groups to be disadvantageous for high speeds and energy efficiency because of its nonlinear loss induced by two-photon absorption (TPA) at telecommunication wavelengths.[1,2] Different materials with wide bandgap energy to suppress TPA at telecommunication wavelengths are proposed and studied for nonlinear integrated optics, including Hydex,[3] Si_3N_4,[4] AlN,[5] Ta_2O_5,[6] TiO_2,[7] SiC,[8] Si_7N_3,[9,10] and AlGaAs.[11]

Recently, silicon carbide has emerged as a promising platform for integrated nonlinear optics because of its large refractive index, Kerr nonlinearity, and wide bandgap. The large bandgap (larger than 2.4 eV[12]) suppresses TPA at telecommunication wavelengths. High confinement in the waveguide core resulting from large refractive index contrast between the silicon carbide (larger than 2.4[12]) and the cladding material (1.44), combined with high Kerr nonlinearity (on the order of 10^{-15} cm^2/W[13,14]), leads to a high nonlinear parameter (γ) for the waveguide. The most extensively studied silicon carbides are 3C SiC, 4H SiC, and 6H SiC, on which different devices such as microdisk cavities,[15,16] ring resonators,[17,18] and photonic crystal cavities[19,20] are investigated for applications in linear and nonlinear integrated optics. In addition, single photon emitters utilizing point defects in SiC make it a promising platform for quantum optics.[21–24] In our previous work,[8] we proposed PECVD amorphous-silicon carbide (a-SiC) on SiO_2 as a platform for integrated nonlinear optics. a-SiC exhibits a linear refractive index of 2.45 and a higher Kerr nonlinearity of 4.8×10^{-14} cm^2/W at telecommunication wavelengths. With a bandgap of 2.3 eV, TPA is also absent. The PECVD deposition temperature of 300 °C makes it compatible with CMOS processes. Moreover, PECVD a-SiC, which can be directly deposited on an insulator layer of a lower refractive index offers easier fabrication processing than crystalline SiC.

In integrated nonlinear optics, four wave mixing (FWM) processes are fundamental to various applications, including wavelength conversion,[11] parametric amplification,[10] signal regeneration,[25] optical demultiplexing,[26] and more. Micro-cavity devices have been used for enhancing the wavelength conversion efficiency (*CE*) of FWM by augmenting the power intensity inside the cavity. Enhanced FWM in SiC ring resonators has been demonstrated before.[13,14] However, limited by the low quality factor and high waveguide loss, the conversion efficiency is very low, or very high pump power is required to achieve a high conversion efficiency.

In this work, we demonstrate high efficiency four wave mixing in an a-SiC ring resonator with a loaded quality factor of 70 000. A conversion efficiency (*CE*) of −21 dB is achieved with 15 mW input pump power. We further characterize a 35 dB enhancement in CE using the ring resonator, compared to that achieved in a 12 mm long waveguide. Compared with other work, we have achieved higher *CE* with a lower input pump power due to the larger Kerr nonlinearity and higher ring resonator quality factor. In addition, the thermo-optic coefficient (TOC) of amorphous silicon carbide is measured to be 1.4×10^{-4}/°C at 1550 nm. Finally, optical bistability is demonstrated in the same ring resonator.

RESULTS

Following the processes described in Ref. 8, we fabricated cladded a-SiC ring resonators with waveguide cross sections of 350×1000 nm^2. The ring resonator bus waveguide is 12 mm long. The gap between the ring and bus waveguide is 400 nm. Figure 1(a) shows the waveguide cross section of one such etched resonator as a black rectangle with vertical sidewalls.

The ring resonator used for FWM is first characterized using a tunable laser with a low output power, to avoid the thermo-optic (TO) effect, and a normalized transmission spectrum of the TM_0 mode is plotted in Fig. 1(b). By applying a Lorentzian fit to the measurement results, the loaded quality factor of the ring resonator is extracted to be 70 000, corresponding to an intrinsic quality factor of 160 000. The ring resonator is operated in the over-coupled regime, and a waveguide loss of around 3.2 dB/cm is obtained. The free spectral range is 2.7 nm from which the group index of the waveguide is derived to be 2.88 at 1550 nm. Using equation $D = \frac{1}{c}\frac{dn_g}{d\lambda}$, the average waveguide dispersion D in the wavelength region at 1550 nm is calculated to be −2700 ps/km nm, as shown in Fig. 1(c). However, the dispersion of the waveguide can be easily engineered by engineering the geometry of the waveguide. In Fig. 1(d), the simulation results show that anomalous dispersion can be achieved by increasing the waveguide thickness to 600 nm.

The experimental setup for FWM measurements is sketched in Fig. 2. The pump and signal are generated by two continuous-wave (CW) tunable laser sources (TLS). The pump is amplified by an erbium-doped fiber amplifier (EDFA) and combined with the signal using a 50:50 coupler. The light is coupled into and out of the devices using lensed fibers and on-chip inverse tapers. The output

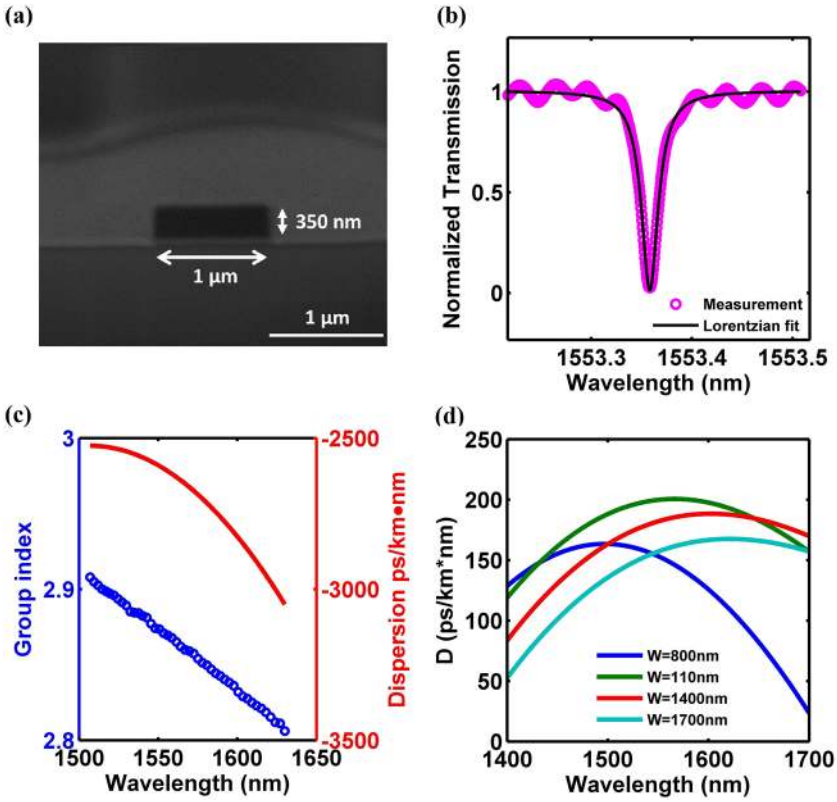

FIG. 1. (a) FIB milled cross section of the cladded a-SiC waveguide with dimensions of 350×1000 nm^2. (b) Transmission spectrum for the ring resonator with 50 μm radius and 350×1000 nm^2 waveguide cross section. Red dots, experimental measurement and black line, Lorentzian fit. The loaded quality factor is 70 000. (c) Group index (blue dots) of waveguide with a dimension of 350×1000 nm^2 extracted from the ring resonator spectrum. Waveguide dispersion (red line) extracted from the group index. (d) Simulation results show that the TM_0 mode of waveguides with 600 nm height and various widths has anomalous dispersion.

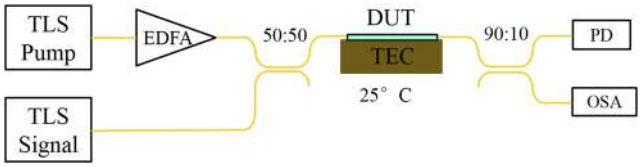

FIG. 2. FWM experimental setup. TLS, tunable laser source; EDFA, erbium-doped fiber amplifier; DUT, devices under test; TEC, thermoelectric cooler; PD, photodetector; and OSA, optical spectrum analyzer.

light is collected into a photodetector (PD) and an optical spectrum analyzer (OSA) using a 90:10 coupler. The PD measures the transmitted power enabling alignment, while the OSA records the FWM transmission spectrum. Both the signal and the pump waves generated by the CW TLS are linearly polarized and aligned to the transverse magnetic (TM) polarization of the waveguide. All the fibers used in the setup are polarization-maintaining optical fibers, ensuring the match of polarizations of both the signal and the pump wave to maximize the conversion efficiency of FWM. The devices under test (DUT) are placed on a thermoelectric cooler (TEC) that is maintained at a constant temperature of 25 °C, thus avoiding a shift in resonance of the ring resonator caused by environmental temperature fluctuations.

Figure 3(a) shows the FWM spectra when the input pump power is 15 mW. For the ring resonator, the FWM *CE* is calculated by the ratio between the on-resonance signal power right before coupling into the ring resonator ($P_{in,signal}$) and the on-resonance idler power coupling out of the ring resonator ($P_{out,idler}$). $P_{in,signal}$ is the same whether it is on-resonance or off-resonance, and it can be calculated by $P_{in,signal} = aP_{output,signal,off}$, in which a is the power attenuation from the ring resonator to the output coupling fiber and $P_{output,signal,off}$ is the off-resonance signal power collected by the output coupling fiber. In addition, $P_{out,idler}$ can be calculated by $P_{out,idler} = aP_{output,idler,on}$, in which $P_{output,idler,on}$ is the on-resonance idler collected by the output coupling fiber. Then, we can get the equation for *CE* as follows:

$$\eta = \frac{P_{out,idler}}{P_{in,signal}} = \frac{P_{output,idler,on}}{P_{output,signal,off}}. \quad (1)$$

As shown in Fig. 3(a), the *CE*, we achieved is −21 dB. Comparing with the previous FWM experimental results with SiC platforms,[13,14] we have achieved a higher *CE* of −21 dB with a lower pump power of 15 mW, owing to the higher quality factor and Kerr nonlinearity of our a-SiC ring resonator.

FWM experiments are also performed in a 12 mm long a-SiC waveguide with the same cross sectional dimensions of 350 × 1000 nm^2, whose results are plotted as blue dots in Fig. 3(b). Comparing the *CE* for the ring resonator (formed by a 314 μm long waveguide) and the 12 mm long waveguide, 35 dB *CE* enhancement is achieved for the ring resonator, as shown in Fig. 3(b).

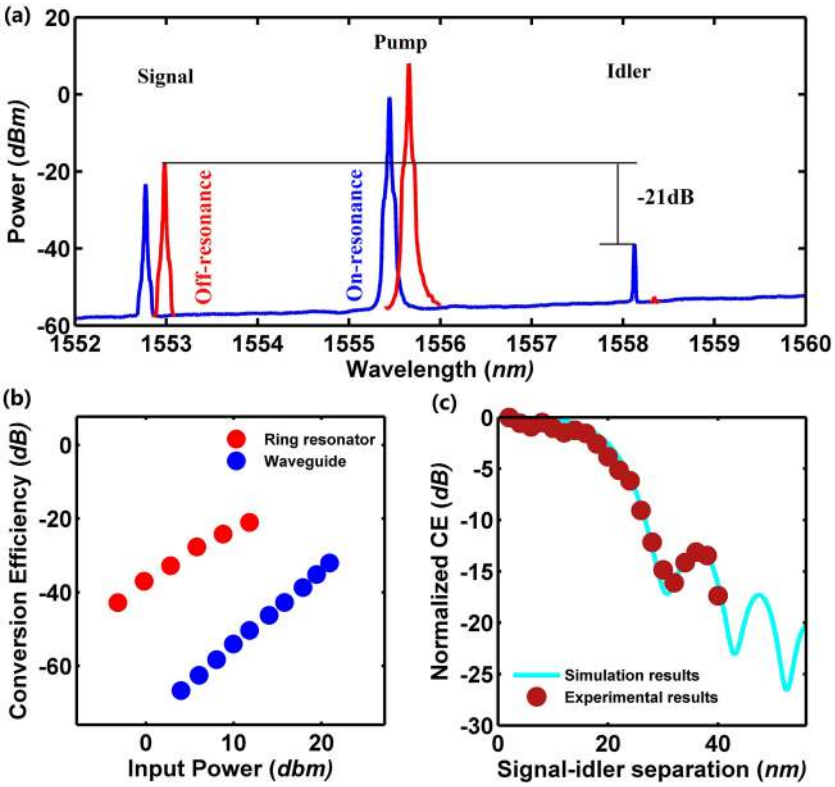

FIG. 3. (a) The ring resonator FWM spectra while both the pump and the signal waves are on-resonance (blue line) and off-resonance (red line). The CE is −21 dB when the input pump power is around 15 mW. (b) CE comparison between the ring resonator with 50 μm radius and the 12 mm long waveguide. 35 dB CE enhancement is achieved. (c) Normalized CE for the waveguide with respect to the signal–idler separation. Simulation results: cyan line and experimental results: red dots. The wavelength conversion bandwidth is 20 nm.

The FWM *CE* for the ring resonator is calculated by[27]

$$CE = \gamma^2 P_p^2 L_{eff}^2 FE_p^4 FE_s^2 FE_i^2, \tag{2}$$

$$L_{eff}^2 = L^2 e^{-\alpha L} \left| \frac{1 - e^{-\alpha L + j\Delta kL}}{\alpha L - j\Delta kL} \right|^2, \tag{3}$$

$$FE = \left| \frac{\kappa}{1 - \tau e^{-\alpha L/2 + j\Delta kL}} \right|, \tag{4}$$

where γ is the waveguide nonlinear parameter. P_p is the pump power, and L_{eff} is the effective length of waveguide. L is the circumference of the ring. α is the waveguide loss. Δk is the phase mismatch defined as $2k_p - k_s - k_i$, where k_p, k_s, and k_i are the propagation constants of the pump, signal, and idler inside the waveguide, respectively. *FE* is the field enhancement factor inside the ring resonator. κ and τ are related by the expression, $|\kappa|^2 + |\tau|^2 = 1$, and refer to the ring's coupling and transmission coefficients, respectively. Compared with a waveguide whose conversion efficiency is determined by $CE = \gamma^2 P_p^2 L_{eff}^2$, the *CE* of the ring resonator is enhanced by the factor of *FE*.[8] For our ring resonator, while the phase mismatch is 0 in the case that both the signal and the idler are placed very close to the pump, the field enhancement *FE* is calculated to be 6.3, leading to 40 times power enhancement in the ring resonator. This explains the 35 dB CE enhancement in the 314 μm long ring resonator compared to the 12 mm long normal waveguide.

It is also observed in Fig. 3(b) that the *CE* saturates slightly with the pump power. In our previous work,[8] we find that the three photon absorption is only noticeable while the light power is more than several watts. In this work, the maximum pump power is only 15 mW, whereas the maximum power in the ring resonator is less than 1 W when considering the resonator enhancement effect. So this slight saturation should not be caused by three photon absorption. In the experiments, while the pump power is high, we were not able to locate the pump exactly on resonance due to the instability caused by the thermo-optic effect. Thus, all three wavelengths are not exactly on resonance, causing the field enhancement factor to be lower compared to that at a lower pump power. As a result, a slight saturation of *CE* is observed with the pump power.

FWM wavelength conversion bandwidth in the waveguide is also analyzed by measuring *CE* as a function of signal–idler separation in a 12 mm long waveguide with dimensions of 350 × 1000 nm^2. For these experiments, the pump wavelength is fixed at 1550 nm and the *CE* is measured, while the signal wavelength is tuned away from the pump wavelength. As shown in Fig. 3(c), the experimental results have a very good match with the simulation results. In Fig. 3(c), a decrease in the *CE* is observed as the signal–idler separation increases from 0 nm to 30 nm. The 3 dB conversion bandwidth is around 20 nm. Since the waveguide exhibits very strong normal dispersion (−3000 ps/km nm), the *CE* at larger signal–idler detuning is eliminated by the large phase mismatch arising from strong normal dispersion, as expressed in Eqs. (2)–(4). When the signal–idler detuning exceeds 30 nm, an increase in *CE* is observed. This is caused by the presence of higher order dispersion, which serves to reduce the phase mismatch.

We continue our experiments to characterize the TOC of a-SiC by measuring the temperature induced spectral shift of the ring resonator's resonance. The same a-SiC ring resonator and TM_0 mode as the FWM experiments are used. Figure 4(a) shows the ring resonator spectra measured at different temperatures ranging from 25 °C to 45 °C; the red shift in the resonant wavelength with temperature implies a positive TOC for a-SiC. By extracting the data from Fig. 4(a), the resonant wavelength of the ring resonator at different temperatures is plotted in Fig. 4(b). From the linear fit to data in Fig. 4(b), we get the spectral shift in response to temperature change, $d\lambda/dT$ = 0.0627 nm/°C for the ring resonator. The relationship between the spectral shift with temperature $d\lambda/dT$ and the effective index change, dn_{eff}/dT may then be extracted as follows:[28]

$$\frac{d\lambda}{dT} = \left(a n_{eff} + \frac{dn_{eff}}{dT} \right) \frac{\lambda}{n_g}, \tag{5}$$

where $a = 2.6 \times 10^{-6}$/°C is the expansion coefficient of the silicon dioxide substrate in response to the temperature change, $n_{eff} = 1.83$ is the effective index of the waveguide, and $n_g = 2.88$ is the group index of the waveguide at 1550 nm. It follows from Eq. (5), that dn_{eff}/dT for the waveguide is 1.12×10^{-4}/°C. dn_{eff}/dT is calculated in COMSOL simulation using TOC of a-SiC as a fitting parameter. We extract the TOC using the measured value of dn_{eff}/dT (1.12×10^{-4}/°C). The calculated TOC of a-SiC is around 1.4×10^{-4}/°C

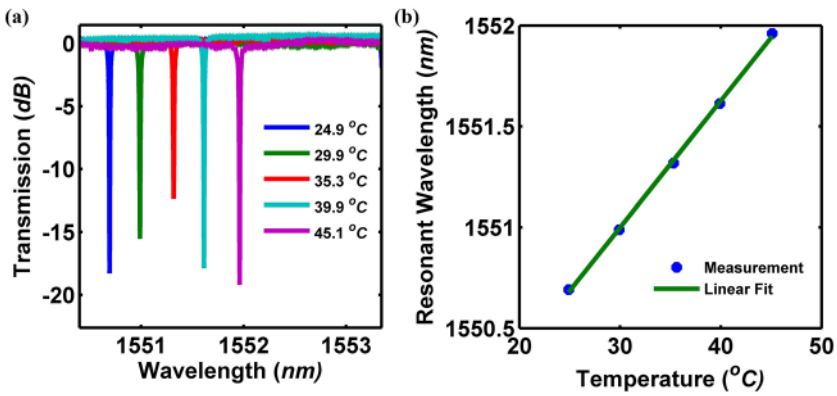

FIG. 4. (a) Spectral shift of the ring resonator in response to temperature change around 1550 nm. As the temperature is increased gradually, the ring resonator's resonance has a red shift. (b) Measured ring resonator resonance wavelength with respect to temperature. Blue dots are the experimental data extracted from (a), and the green line is the linear fit, which allows us to extract a value of $d\lambda/dT$ = 0.0627 nm/°C.

at a wavelength of 1550 nm, which is slightly higher compared to a previously reported value.[29] This can be the result of different deposition conditions and, therefore, the composition of the a-SiC films. In this measurement, the uncertainty in the measured waveguide dimension is around ±10 nm, resulting in an uncertainty of $\pm 0.05 \times 10^{-4}/^{\circ}C$ for TOC of a-SiC.

Taking advantage of the high TOC of the a-SiC, we demonstrate optical bistability in the a-SiC ring resonator. Ring resonator device parameters used in the FWM experiments are used for the demonstration of optical bistability. In addition, the TM_0 mode is used. The power-dependent transmission spectrum of the ring resonator is measured using a tunable laser source at different laser output powers. The tunable laser wavelength is scanned in two opposite directions—up-scan and down-scan directions. The up-scan direction means the wavelength is scanned from blue side to the red side of the resonance wavelength, while the down-scan direction is opposite. The spectra of the ring resonator for the two opposite directions with different laser powers are plotted in Fig. 5(a); The spectra measured in the up-scan and down-scan directions are plotted using solid and dashed lines, respectively. When the laser power is very low, the spectra of two scan directions are the same. However, when the laser power is higher, the difference between the two spectra becomes larger. It is observed that, for some wavelengths, the transmitted power is different for two opposite scan directions. In many popular platforms for integrated optics such as silicon, the optical bistability may be a combined result of the thermo-optic effect and the free carrier dispersion effect.[30,31] However, in the a-SiC, TPA is absent. So the optical bistability is mainly caused by the thermo-optic effect. In the up-scan mode, with the tuning of the wavelength toward the resonance, light is coupled into the ring resonator and this causes the temperature of the ring resonator to increase. As the optical wavelength approaches the resonance wavelength, more heat is introduced inside the ring resonator, causing a red shift of the resonance wavelength. The closer the laser wavelength is to the resonance wavelength, the greater the extent of the resonance red shift. There is one point where the laser wavelength is exactly on resonance and the transmission is minimum in the spectrum. Once the light wavelength exceeds this point, the laser wavelength is not on resonance any more. The light intensity and the heat inside the ring resonator will decrease, causing a blue shift of the resonance wavelength. The blue shift of the resonance causes the laser wavelength to move further out of resonance. As a result, the ring resonator temperature will further decrease, causing a further blue shift of the resonance. Finally, the laser wavelength will be totally off resonance, resulting in close to 100% transmission in the spectrum. As shown in Fig. 5(b), when the input power increases from 0.2 mW to 2 mW, the resonance wavelength increases from 1550.7 nm to 1550.8 nm with a resonance shift rate of 58.3 pm/mW, as a result of a-SiC's positive TOC.

CONCLUSION

In this work, we fabricate PECVD-deposited amorphous SiC with a loaded quality factor of 70 000, in which high efficiency wavelength conversion via FWM is demonstrated. A conversion efficiency of −21 dB is achieved with a pump power of 15 mW. Due to the high quality factor of the ring resonator (70 000) and high Kerr nonlinearity (4.8×10^{-14} cm^2/W) of a-SiC, we achieved the highest wavelength conversion efficiency on a SiC platform, despite using a low pump power. In addition, by measuring the spectral shift in response to temperature change, the TOC of a-SiC is extracted to be $1.4 \times 10^{-4}/^{\circ}C$ at a wavelength of 1550 nm. Finally, optical bistability is demonstrated in the ring resonator.

The a-SiC platform with high Kerr nonlinearity and low loss is sought after for another interesting application—optical parametric oscillator (OPO). Two main limitations for achieving OPO on a-SiC are studied carefully. One limitation is the normal dispersion. However, as we discussed earlier, anomalous dispersion can be achieved for the waveguide with 600 nm thickness. Another limitation is the existence of three-photon absorption. The three-photon absorption in our deposited a-SiC films was previously characterized to be ~0.01 cm^3/GW^2 at the 1550 nm region.[8] There is no two-photon absorption. Silicon is dominated by two-photon absorption at 1550 nm and is, therefore, not ideal for oscillation. We compare the three-photon absorption of amorphous silicon carbide with that of AlGaAs, where the three-photon absorption coefficient has been characterized to be ~0.04 cm^3/GW^2,[32] and parametric oscillation has been shown to be possible.[33,34] Our a-SiC films have four times lower three-photon absorption coefficient than AlGaAs. Consequently, the three-photon absorption coefficient should not be a showstopper for achieving oscillation.

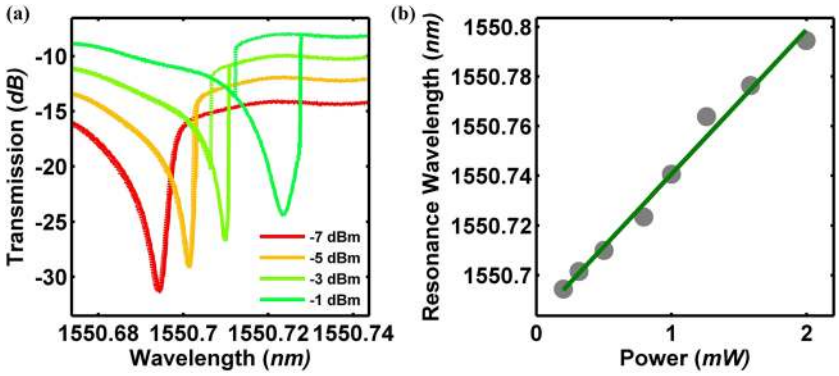

FIG. 5. (a) Spectra of the ring resonator for two opposite scan directions with different laser input powers. The solid line represents the up-scan direction spectra and dashed line represents the down-scan direction spectra. (b) Resonance wavelength shift with an increase in the input laser power. The gray dots are the experimental results. The resonance shift rate is extracted using the linear fit to the experimental data (green line) to be 58.3 pm/mW.

To sum up, this work shows the great potential of a-SiC for applications in CMOS-compatible, on-chip optical signal processing.

ACKNOWLEDGMENTS

Funding from the National Research Foundation Competitive Research (Grant No. NRF-CRP18-2017-03) and A*STAR-NTU-SUTD AI Partnership grant is gratefully acknowledged.

DATA AVAILABILITY

The data that support the findings of this study are available from the corresponding author upon reasonable request.

REFERENCES

[1]H. K. Tsang, C. S. Wong, T. K. Liang, I. E. Day, S. W. Roberts, A. Harpin, J. Drake, and M. Asghari, "Optical dispersion, two-photon absorption and self-phase modulation in silicon waveguides at 1.5 μm wavelength," Appl. Phys. Lett. **80**, 416 (2002).

[2]A. D. Bristow, N. Rotenberg, and H. M. van Driel, "Two-photon absorption and Kerr coefficients of silicon for 850–2200 nm," Appl. Phys. Lett. **90**, 191104 (2007).

[3]L. Razzari, D. Duchesne, M. Ferrera, R. Morandotti, S. Chu, B. E. Little, and D. J. Moss, "CMOS-compatible integrated optical hyper-parametric oscillator," Nat. Photonics **4**, 41 (2010).

[4]J. S. Levy, A. Gondarenko, M. A. Foster, A. C. Turner-Foster, A. L. Gaeta, and M. Lipson, "CMOS-compatible multiple-wavelength oscillator for on-chip optical interconnects," Nat. Photonics **4**, 37 (2010).

[5]H. Jung, C. Xiong, K. Y. Fong, X. Zhang, and H. X. Tang, "Optical frequency comb generation from aluminum nitride microring resonator," Opt. Lett. **38**, 2810 (2013).

[6]C.-L. Wu, Y.-J. Chiu, C.-L. Chen, Y.-Y. Lin, A.-K. Chu, and C.-K. Lee, "Four-wave-mixing in the loss low submicrometer Ta_2O_5 channel waveguide," Opt. Lett. **40**, 4528 (2015).

[7]X. Guan, H. Hu, L. K. Oxenløwe, and L. H. Frandsen, "Compact titanium dioxide waveguides with high nonlinearity at telecommunication wavelengths," Opt. Express **26**, 1055 (2018).

[8]P. Xing, D. Ma, K. J. A. Ooi, J. W. Choi, A. M. Agarwal, and D. Tan, "CMOS-compatible PECVD silicon carbide platform for linear and nonlinear optics," ACS Photonics **6**, 1162 (2019).

[9]T. Wang, D. K. T. Ng, S.-K. Ng, Y.-T. Toh, A. K. L. Chee, G. F. R. Chen, Q. Wang, and D. T. H. Tan, "Supercontinuum generation in bandgap engineered, back-end CMOS compatible silicon rich nitride waveguides," Laser Photonics Rev. **9**, 498 (2015).

[10]K. J. A. Ooi, D. K. T. Ng, T. Wang, A. K. L. Chee, S. K. Ng, Q. Wang, L. K. Ang, A. M. Agarwal, L. C. Kimerling, and D. T. H. Tan, "Pushing the limits of CMOS optical parametric amplifiers with UUSRN: Si_7N_3 above the two-photon absorption edge," Nat. Commun. **8**, 13878 (2017).

[11]M. Pu, H. Hu, L. Ottaviano, E. Semenova, D. Vukovic, L. K. Oxenløwe, and K. Yvind, "Ultra-efficient and broadband nonlinear AlGaAs-on-insulator chip for low-power optical signal processing," Laser Photonics Rev. **12**, 1800111 (2018).

[12]G. L. Harris, *Properties of Silicon Carbide* (INSPEC, the Institution of Electrical Engineers, London, UK, 1995).

[13]F. Martini and A. Politi, "Four wave mixing in 3C SiC ring resonators," Appl. Phys. Lett. **112**, 251110 (2018).

[14]Y. Zheng, M. Pu, A. Yi, X. Ou, and H. Ou, "4H-SiC microring resonators for nonlinear integrated photonics," Opt. Lett. **44**, 5784 (2019).

[15]X. Lu, J. Y. Lee, P. X.-L. Feng, and Q. Lin, "High Q silicon carbide microdisk resonator," Appl. Phys. Lett. **104**, 181103 (2014).

[16]D. Allioux, A. Belarouci, D. Hudson, E. Magi, M. Sinobad, G. Beaudin, A. Michon, N. Singh, R. Orobtchouk, and C. Grillet, "Toward mid-infrared nonlinear optics applications of silicon carbide microdisks engineered by lateral under-etching [invited]," Photonics Rev. **6**, B74–B81 (2018).

[17]F. Martini and A. Politi, "Linear integrated optics in 3C silicon carbide," Opt. Express **25**, 10735 (2017).

[18]J. Cardenas, M. Zhang, C. T. Phare, S. Y. Shah, C. B. Poitras, B. Guha, and M. Lipson, "High Q SiC microresonators," Opt. Express **21**, 16882 (2013).

[19]M. Radulaski, T. M. Babinec, S. Buckley, A. Rundquist, J. Provine, K. Alassaad, G. Ferro, and J. Vučković, "Photonic crystal cavities in cubic (3C) polytype silicon carbide films," Opt. Express **21**, 32623 (2013).

[20]D. O. Bracher and E. L. Hu, "Fabrication of high-Q nanobeam photonic crystals in epitaxially grown 4H-SiC," Nano Lett. **15**, 6202 (2015).

[21]M. Radulaski, M. Widmann, M. Niethammer, J. L. Zhang, S.-Y. Lee, T. Rendler, K. G. Lagoudakis, N. T. Son, E. Janzén, T. Ohshima, J. Wrachtrup, and J. Vučković, "Scalable quantum photonics with single color centers in silicon carbide," Nano Lett. **17**, 1782 (2017).

[22]J. Wang, Y. Zhou, Z. Wang, A. Rasmita, J. Yang, X. Li, H. J. Bardeleben, and W. Gao, "Bright room temperature single photon source at telecom range in cubic silicon carbide," Nat. Commun. **9**, 4106 (2018).

[23]J. Wang, X. Zhang, Y. Zhou, K. Li, Z. Wang, P. Peddibhotla, F. Liu, S. Bauerdick, A. Rudzinski, Z. Liu, and W. Gao, "Scalable fabrication of single silicon vacancy defect arrays in silicon carbide using focused ion beam," ACS Photonics **4**, 1054 (2017).

[24]D. M. Lukin, C. Dory, M. A. Guidry, K. Y. Yang, S. D. Mishra, R. Trivedi, M. Radulaski, S. Sun, D. Vercruysse, G. H. Ahn, and J. Vučković, "4H-silicon-carbide-on-insulator for integrated quantum and nonlinear photonics," Nat. Photonics **14**, 330 (2019).

[25]R. Salem, M. A. Foster, A. C. Turner, D. F. Geraghty, M. Lipson, and A. L. Gaeta, "Signal regeneration using low-power four-wave mixing on silicon chip," Nat. Photonics **2**, 35 (2008).

[26]F. Li, M. Pelusi, D.-X. Xu, A. Densmore, R. Ma, S. Janz, and D. J. Moss, "Error-free all-optical demultiplexing at 160 Gb/s via FWM in a silicon nanowire," Opt. Express **18**, 3905 (2010).

[27]P. P. Absil, J. V. Hryniewicz, B. E. Little, P. S. Cho, R. A. Wilson, L. G. Joneckis, and P.-T. Ho, "Wavelength conversion in GaAs micro-ring resonators," Opt. Lett. **25**, 554 (2000).

[28]F. Qiu, A. M. Spring, and S. Yokoyama, "Athermal and high-Q hybrid TiO_2–Si_3N_4 ring resonator via an etching-free fabrication technique," ACS Photonics **2**, 405 (2015).

[29]F. G. D. Corte, M. E. Montefusco, L. Moretti, I. Rendina, and A. Rubino, "Study of the thermo-optic effect in hydrogenated amorphous silicon and hydrogenated amorphous silicon carbide between 300 K and 500 K at 1.55 μm," Appl. Phys. Lett. **79**, 168 (2001).

[30]V. R. Almeida and M. Lipson, "Optical bistability on a silicon chip," Opt. Lett. **29**, 2387 (2004).

[31]Q. Xu and M. Lipson, "Carrier-induced optical bistability in silicon ring resonators," Opt. Lett. **31**, 341 (2006).

[32]J. U. Kang, A. Villeneuve, M. Sheik-Bahae, G. I. Stegeman, K. Al-hemyari, J. S. Aitchison, and C. N. Ironside, "Limitation due to three-photon absorption on the useful spectral range for nonlinear optics in AlGaAs below half band gap," Appl. Phys. Lett. **65**, 147 (1994).

[33]M. Pu, L. Ottaviano, E. Semenova, and K. Yvind, "Efficient frequency comb generation in AlGaAs-on-insulator," Optica **3**, 823–826 (2016).

[34]L. Chang, W. Xie, H. Shu *et al.*, "Ultra-efficient frequency comb generation in AlGaAs-on-insulator microresonators," Nat. Commun. **11**, 1331 (2020).